Ground-based remote sensing of atmospheric total column CO_2 and CH_4 by direct sunlight in Hefei*

Cheng Si-Yang(程巳阳), Xu Liang(徐 亮)†, Gao Min-Guang(高闽光), Li Sheng(李 胜), Jin Ling(金 岭), Tong Jing-Jing(童晶晶), Wei Xiu-Li(魏秀丽), Liu Jian-Guo(刘建国), and Liu Wen-Qing(刘文清)

Key Laboratory of Environment Optics & Technology, Anhui Institute of Optics and Fine Mechanics, Chinese Academy of Sciences, Hefei 230031, *China*

(Received 20 March 2013; revised manuscript received 15 May 2013)

Fourier transform spectrometry has played an important role in the three-dimensional greenhouse gas monitoring as the focus of attention on global warming in the past few years. In this paper, a ground-based low-resolution remote sensing system measuring the total columns of CO_2 and CH_4 is developed, which tracks the sun automatically and records the spectra in real-time and has the advantages of portability and low cost. A spectral inversion algorithm based on nonlinear least squares spectral fitting procedure for determining the column concentrations of these species is described. Atmospheric transmittance spectra are computed line-by-line in the forward model and observed on-line by direct solar radiation. Also, the wavelength shifts are introduced and the influence of spectral resolution is discussed. Based on this system and algorithm, the vertical columns of O_2, CO_2, and CH_4 are calculated from total atmospheric observation transmittance spectra in Hefei, and the results show that the column averaged dry-air mole fractions of CO_2 and CH_4 are measured with accuracies of 3.7% and 5%, respectively. Finally, the H_2O columns are compared with the results observed by solar radiometer at the same site and the calculated correlation coefficient is 0.92, which proves that this system is suitable for field campaigns and used to monitor the local greenhouse gas sources under the condition of higher accuracy, indirectly.

Keywords: carbon dioxide, methane, ground-based remote sensing, solar absorption spectroscopy

PACS: 92.30.Np, 42.68.Wt, 42.68.Ca **DOI:** 10.1088/1674-1056/22/12/129201

1. Introduction

The global network of the high-resolution ground-based Fourier transform spectrometer (FTS) built for providing long-term spectroscopic observations of greenhouse gases in the terrestrial atmosphere has been used successfully not only for trend analysis, but also for the validation of satellite experiments.[1,2] In contrast, global satellite measurement of the greenhouse gas column has provided a better spatiotemporal distribution of greenhouse gas sources and sinks with poorer precision.[3,4] *In situ* instruments located on an airplane or installed at a terrestrial station were also used to monitor greenhouse gas concentration with high accuracy and sparse spatial coverage.[5,6] In turn, the ground-based FTS in the near infrared region measured the same quantity (column concentrations) as the satellite and the data observed by the satellite were shown to have less temporal variability than *in-situ* data which were directly influenced by local flux.[7,8] The column averaged dry-air mole fraction of CH_4, named XCH_4, can now be measured with an accuracy of better than 0.4% and XCO_2 (the column averaged dry-air mole fraction of CO_2) to be better than 0.25% by ground-based high-resolution FTS.[9]

However, not all great ideas are free of problems and challenges. The CO_2 mean annual concentration at Mauna Loa only increased at an average rate of 1.37×10^{-6}/year from 315×10^{-6} in 1958 to 381×10^{-6} in 2006 with the primary anthropogenic contribution.[10] It was very important to obtain high-quality solar absorption spectra in the near-infrared region and inverse the spectra with the appropriate radiation transfer model and algorithm. Although the high-resolution FTS could meet this need, it was enormous and required a specific laboratory. By contrast, low-resolution FTS could easily be used for short-term campaigns or in remote areas.

In this paper, in Section 2, briefly described is a home-made system of low-resolution ground-based FTS recording spectra in Hefei continuously.[11–14] A nonlinear least squares spectral inversion algorithm is presented and the column concentrations of greenhouse gases are inversed from total atmospheric transmittance in Section 3. Meanwhile, the processing of wavelength shifts is introduced. In Section 4, the influence of spectral resolution is discussed, and column averaged dry-air mole fractions of CO_2 and CH_4 are measured with accuracies of 3.7% and 5%, respectively. In addition, we verify the validity by comparing H_2O column with the data measured by other instruments at the same site.

*Project supported by the National Key Technology Research and Development Program of the Ministry of Science and Technology of China (Grant No. 2012BAJ24B02) and the National Natural Science Foundation of China (Grant Nos. 40905011 and 41105022).

†Corresponding author. E-mail: xuliang@aiofm.ac.cn

© 2013 Chinese Physical Society and IOP Publishing Ltd

2. Instrumentation

A low-resolution ground-based Fourier transform infrared spectrometer (LRFTS) was installed in a house on the roof at our institute. As shown in Fig. 1, it mainly contains six parts: weather station, sun-tracker, skylight, Michelson interferometer, wireless antenna, and micro-computer. The weather station was mounted on the southeast side of the house about 15 meters from the ground. The home-made sun-tracker, driven by a quadrant detector, was installed near the skylight in the house. It tracks the sun and feeds a parallel light beam into the Michelson interferometer by inserting a flat mirror at 45° into the vertical light beam. Spectra were recorded by the Michelson interferometer at a maximum resolution of 1 cm^{-1}. This instrument was equipped with CaF_2 beam splitter and indium gallium arsenide (InGaAs) infrared (IR) detector, cooled by electricity and covering 5400 cm^{-1}~9000 cm^{-1}. A wireless antenna was used to deliver data and receive long-distance commands. A micro-computer was used to save data and control system operation.

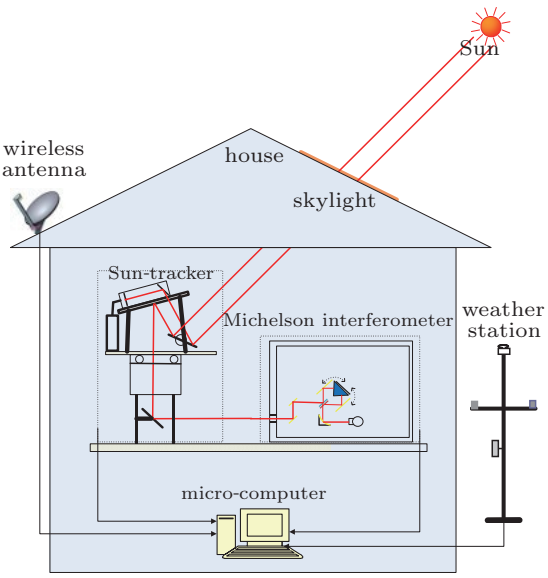


Fig. 1. (color online) Schematic diagram of observation system.

3. Inversion of the spectra

The spectral inversion algorithm provides volume-mixing ratios (VMRs) of greenhouse gases,[15] such as CO_2 and CH_4, averaged between the Sun and the instrument. This is achieved through nonlinear least squares (NLLS) spectral fitting procedure applied to the total atmospheric transmittance spectra in the backward model. The inversion procedure seeks a best fitting of the observed (T_i^{M}) and modeled (T_i^{C}) transmittance spectra such that the percent root-mean-square (%RMS) is minimized by scaling a priori VMR profile with a single multiplicative factor over all layers. The %RMS is expressed as

$$\%\mathrm{RMS} = 100 \times \sqrt{\frac{\sum_{i=1}^{m} (T_i^{\mathrm{M}} - T_i^{\mathrm{C}})^2}{m}}, \tag{1}$$

where m is the number of spectral points. The quantity $(T_i^{\mathrm{M}} - T_i^{\mathrm{C}})$ is called the residual.

3.1. Modeled transmittance spectra

The transmittance spectra T_i^{C} are modeled by line-by-line spectroscopic calculations using the 1976 U.S. standard atmosphere model as the input atmospheric state,[16] expressed by

$$T_i^{\mathrm{C}} = T(\upsilon_{\mathrm{i}}) = \exp\Bigg\{ -\sum_{j}^{J}\sum_{k}^{K}\sum_{s}^{S}\{[c_{\mathrm{k}} w_{0_{\mathrm{k,j}}}] \times [R_{s,k,j} F_{s,k,j}(\upsilon_i - \upsilon_{k,j})] n_j l_j\}\Bigg\}, \tag{2}$$

where $w_{0_{k,j}}$ is the a priori VMR of the k-th gas in the j-th atmospheric layer, c_k is a factor multiplied to the a priori VMR profile of the k-th gas, $R_{s,k,j}$ and $F_{s,k,j}$ are the absorption strength and the normalized line shape function, respectively, of the s-th line of the k-th gas in the j-th atmospheric layer, $\upsilon_{k,j}$ is the wave-number center of the k-th gas in the j-th layer, n_j is the number density of absorbers in the j-th layer, and l_j is the effective radiation path length in the j-th layer. The spectroscopic line parameters used in this model are cited from the high resolution transmission molecular absorption database (HITRAN) 2004. The pressure and temperature profiles were obtained from the weather station and the atmospheric model. In this paper, we mainly focus on CO_2 and CH_4, identified as the first and second most important greenhouse gases. The O_2 total column, retrieved at 7885-cm^{-1} band, will be used to overcome the common systematic deviations in CO_2 and CH_4 total column caused by air mass errors and so on. Central wave-number and interfering gases are listed in Table 1.

Table 1. Positions for each gas in near infrared solar absorption spectra.

Gas	Central wave-number (υ/cm^{-1})	Interfering gas(es)
O_2	7885.0	H_2O
CO_2	6220.0	H_2O, HDO, CH_4
CH_4	6002.0	CO_2, H_2O, HDO
	6076.0	CO_2, H_2O, HDO

3.2. Observed transmittance spectra

The irradiance spectra are directly influenced by the solar absorption lines and spectral response of the LRFTS so that it is critical to obtain observed total-column transmittance spectra, including the concentration information of greenhouse gases in the atmosphere. The calculation procedure from the irradiance spectrum, shown in Fig. 2, to transmittance is described in detail in the following.[17]

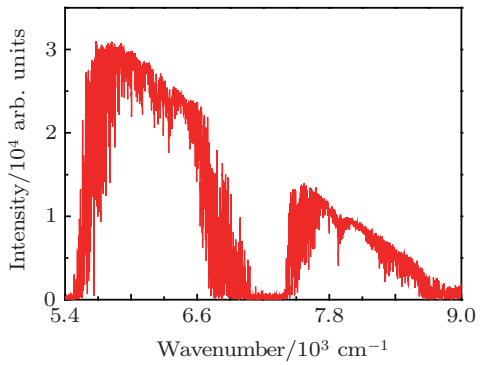


Fig. 2. (color online) Measured single spectrum.

Firstly, the variations of environmental temperature at the observation and solar position make a measured wavelength drift with respect to a reference spectrum. We determine the spectral shift using a spectral extreme point, judging whether its position is consistent with the one in the reference spectrum each time. If not consistent, the absorption spectrum as a whole will be adjusted by the spectral shift.

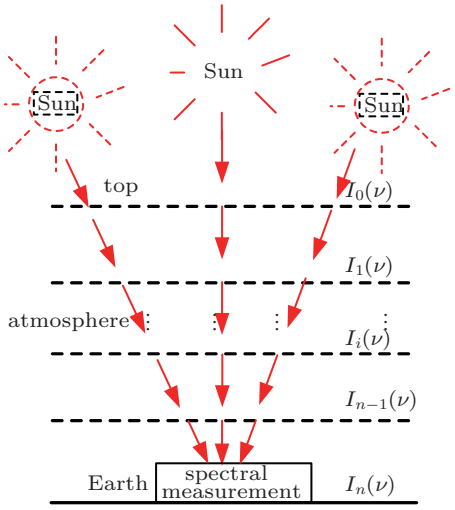


Fig. 3. (color online) Schematic drawing of plane-parallel atmosphere model.

Then, at a given position of the Sun, it is denoted by the solar zenith angle (θ). Consider an atmosphere consisting of plane-parallel layers, shown in Fig. 3. On the basis of the Beer–Lambert law, the irradiance F_{mv} of the direct solar radiation of frequency ν observed at the surface level is given by

$$F_{mv} = F_{ov}\exp[-\varepsilon_\nu \cdot m(\theta)], \tag{3}$$

where F_{ov} is the monochromatic solar irradiance at the top of the atmosphere, ε_ν denotes the monochromatic optical thickness at the zenith direction, $m(\theta)$ represents the ratio of the air mass between the Sun and the observer to the air mass with respect to the local zenith distance. We define the monochromatic transmittance T_{mv} as follows:

$$\begin{aligned} T_{mv} &= F_{mv}/F_{ov} \\ &= \exp[-\varepsilon_\nu \cdot m(\theta)]. \end{aligned} \tag{4}$$

The signal value P_{mv} detected by LRFTS is proportional to the solar irradiance. Define response value P_{ov} corresponding to solar irradiance at the top of the atmosphere. The parameter C_ν is a scale factor. Thus, Eq. (3) can be expressed by

$$\begin{aligned} P_{mv} &= C_\nu F_{ov}\exp[-\varepsilon_\nu \cdot m(\theta)] \\ &= P_{ov}\exp[-\varepsilon_\nu \cdot m(\theta)]. \end{aligned} \tag{5}$$

Taking the logarithm, Eq. (5) is given by

$$\ln[P_{mv}] = \ln[P_{ov}] - \varepsilon_\nu \cdot m(\theta). \tag{6}$$

On the weather condition that the structure of the atmospheric layer is stable and the content of the aerosol is limited, ε_ν is approximately constant. Observations of P_{mv} may be made for several zenith angles during a single day. With respect to noises, a plot of $\ln[P_{mv}]$ versus $m(\theta)$ may be extrapolated to the zero point by the least square method and then $\ln[P_{mv}]$ represents $\ln[P_{ov}]$ at the top of the atmosphere ($m(\theta) = 0$). The quantity P_{ov} is comprised of the solar constant and instrumental constant in common. Actually, the atmospheric transmittance can be calculated, as long as P_{mv} has been measured at a certain time of a clear day, by the formula as follows:

$$T_{mv} = P_{mv}/P_{ov}. \tag{7}$$

The foregoing theoretical procedure is the Smithsonian long method which is usually used for determining the solar constant.[18] The total atmospheric transmittances T_m(total) from the observation of the solar irradiance cover the spectral absorption bands of greenhouse gases. For example, figure 4 shows the spectral transmittances T_m(total) (thin solid line), marked with arrows for gases (CO_2, CH_4, O_2).

The inversion is only sensitive to the relative depth of the absorption line in the spectrum.[19] So the quantity T_m(total) will be divided into two parts: the line absorption T_m(gas) of gas with which the inversion (thick solid line in Fig. 4) can be done and continuum component R_m can be described by a low order polynomial (dashed line in Fig. 4). R_m contains a variety of factors, such as the influences of aerosols and clouds. T_m(gas) is calculated by using the following equation

$$T_m(\text{gas}) \approx T_m(\text{total})/R_m. \tag{8}$$

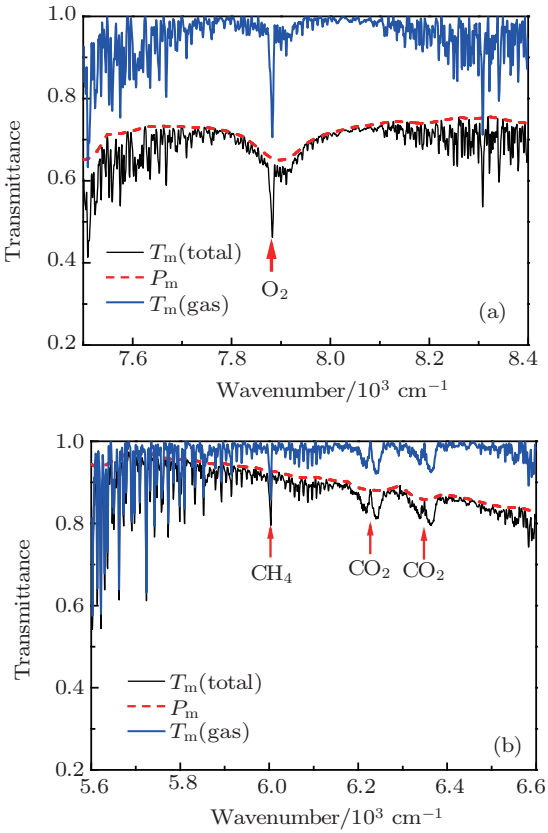


Fig. 4. (color online) Observed spectral transmittances, continuums, and line absorption spectra in different regions (a) 7500 cm^{-1} ~8400 cm^{-1}; (b) 5600 cm^{-1} ~6600 cm^{-1}.

4. Results and discussion

4.1. Spectral resolution

The measurement at a high spectral resolution may show a high sensitivity to atmospheric greenhouse gas change.[20,21] Figure 5 demonstrates the modeled transmittance spectra with different resolutions from 0.016 cm^{-1} to 2 cm^{-1} for three gases (O_2, CO_2, CH_4). Obviously, low-resolution spectra have fewer data points to represent the spectral line, causing different line depth and line width. For 1-cm^{-1} resolution, the individual lines are not resolved and the curvature of the whole spectral analysis region dominates the fitting process. The inversions of total column concentrations for different gases are based on this resolution in the following.

4.2. Spectral fitting

Figure 6 shows an example of spectral fittings for the 7885-cm^{-1} O_2 band, the 6220-cm^{-1} CO_2 band, and the 6002-cm^{-1} CH_4 band, respectively. The largest discrepancies of a few percent between the measured and the modeled transmittances are observed in the vicinity of the absorption line centers. They usually arise from defects in the spectroscopic parameters (line intensity and line width). Also, the residuals are contributed to by sources of error such as imperfect a priori VMR profile and vertical distribution of temperature or humidity. In the non-absorption regions, the residuals are attributed to measurement noise, appearing in a fully random manner. The values of %RMS are 0.85%, 0.62%, and 0.62% in Fig. 6 for the components mentioned above, respectively. The fitting result is satisfying, although they are subjected to interference by water–vapor absorption lines. The value of %RMS for O_2 is larger than that for CO_2 or CH_4 which can be explained as the wider fitting spectral region.

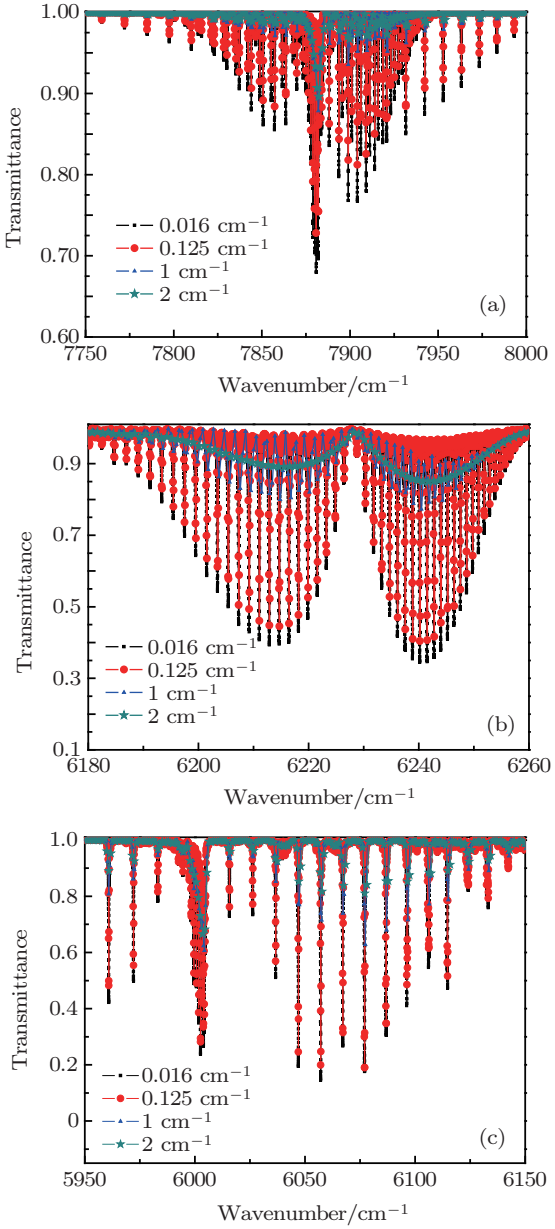


Fig. 5. (color online) Modeled transmittance spectra with resolutions of 0.016, 0.125, 1, and 2 cm^{-1} for different gases (a) O_2; (b) CO_2; (c) CH_4.

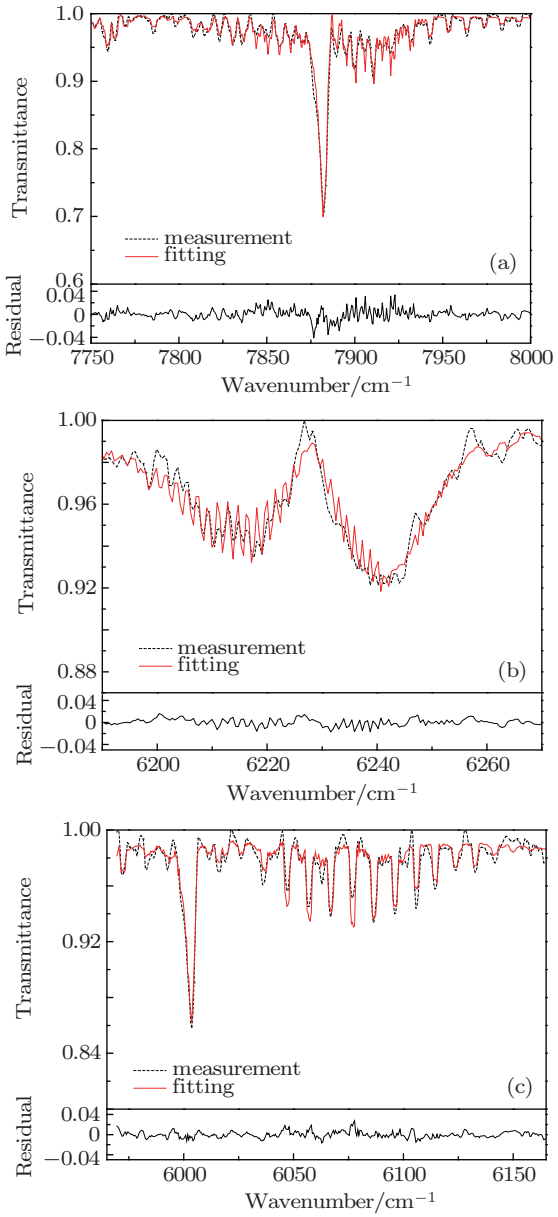


Fig. 6. (color online) Measured transmittance spectra, fitting spectra, and residual spectra about different spectral regions of different gases: (a) O_2, (b) CO_2, and (c) CH_4.

4.3. Retrievals

Figure 7 shows the vertical O_2, CO_2, and CH_4 columns on 15 September 2012. The scattering of the data is caused by low signal-to-noise ratio of the spectrum sampled with a single scan, in which the sharp-changing data points can be removed as a part of post-correction. The sampling error of HeNe reference laser and the temperature differences between inside and outside the house should be taken into account before the instrument operates in a stable manner, which takes approximately 30 minutes.

The mean of vertical O_2 columns in Fig. 7(a) is 3.8×10^{28} molec./m^2, lower than the values presented by Gisi *et al.*,[22] which increases slowly before 14:30 and then decreases until the end of the experiment. The big variation range of O_2 columns, from 3×10^{28} molec./m^2 to 4.5×10^{28} molec./m^2 except anomalous data-points, is determined by some complicated reasons including the signal-to-noise ratio, the solar zenith angle, the resolution of the system, and instrumental line shape (ILS).[23] However, as a home-built experimental system and a self-developed retrieval method, the O_2 columns offer an internal standard to assess the short-term or long-term stability of this system and retrieval method. Therefore the column-average dry-air mole fractions of Gas (CO_2, CH_4, etc.), named XGas, are determined by normalizing it to the approximate constant of O_2 of 0.2095 in the atmosphere, and the XGas is given as

$$\mathrm{XGas} = \frac{\mathrm{column_{Gas}}}{\mathrm{column_{O_2}}} \times 20.95\%. \tag{9}$$

The means of CO_2 columns in Fig. 7(b) and CH_4 columns in Fig. 7(c) are 6.2×10^{25} molec./m^2 and 3.6×10^{23} molec./m^2, lower than the results reported by Gisi *et al.*[22] and Petri *et al.*,[9] respectively. We are not sure about the origin of these offsets, speculating that the uncertainty of the ILS and the difference between retrieval algorithms play an important role. The higher variability of the CO_2 columns is obvious and the weaker dependence on air-mass in the case of the CH_4 columns can be observed when comparing with the intraday variation of the O_2 columns.

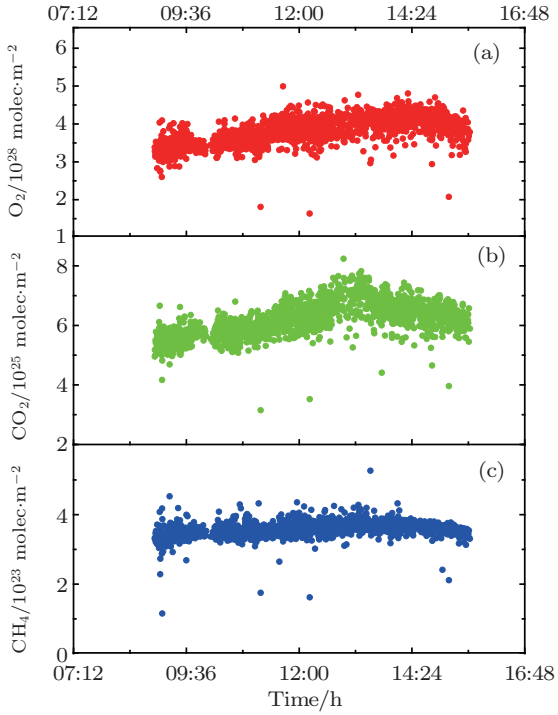


Fig. 7. (color online) Vertical columns of (a) O_2, (b) CO_2, and (c) CH_4 , which were retrieved from observed spectra on 15 September 2012 with NLLS algorithm.

The XCO_2 and XCH_4 values relevant to Fig. 7 and calculated by Eq. (9) are presented in Figs. 8(a) and 8(b), respectively. The mean of XCO_2 in Fig. 8(a) has been shifted

to 385×10^{-6}, based on the estimated value from L2 product about GOSAT (the Greenhouse Gases Observing Satellite).[24] The intraday variability of XCO_2 is different from that of XCH_4, i.e., the former shows an increase before 13:00 and the latter varies very smoothly. To assess the scattering of the data with higher signal-to-noise ratio rather than only one scan, we have applied a running average to the raw XCO_2 and XCH_4, shown in Fig. 8 with solid lines. Then we obtain the accuracies of 3.7% for XCO_2 and 5% for XCH_4 from the following formula:

$$\mathrm{XGas}_{\mathrm{precision}} = \frac{\sigma}{\langle \mathrm{XGas} \rangle} \times 100\%, \tag{10}$$

where $\langle \mathrm{XGas} \rangle$ is the daily mean of XGas, σ is the standard deviation, and $\mathrm{XGas}_{\mathrm{precision}}$ represents the accuracy of XGas.

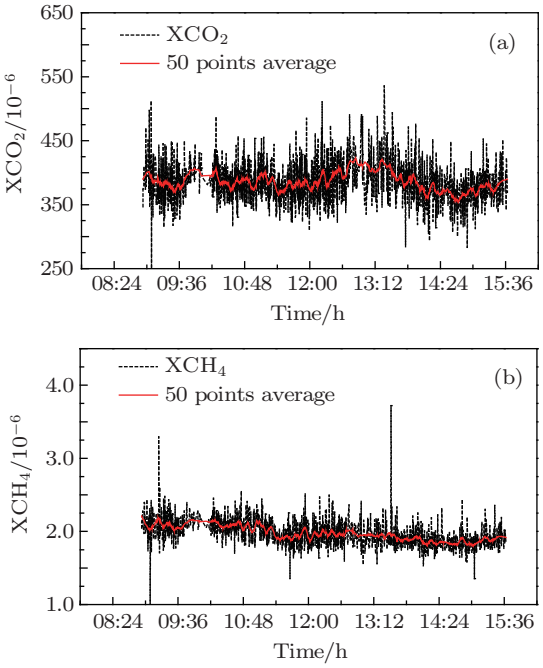


Fig. 8. (color online) Variations of (a) XCO_2 and (b) XCH_4 with time.

4.4. Comparisons

To demonstrate that the results mentioned above are valid, the vertical H_2O columns from our observed spectra are compared with the results measured by solar radiometer (SR) at the same site. The time series of 8 measurement days from 14 September to 14 November 2012 are shown in Fig. 9. The variation of H_2O columns, increasing firstly and then decreasing, is clear during these days, which is useful for comparisons. The means from 14:00 to 15:00 on each measurement day, during which both instruments were operating well and offered valid concentration results, are shown in Fig. 10. Obviously, they have the same trend, although the absolute values are discrepant on some days. As shown in Fig. 11, the correlation coefficient is 0.92 based on the data in Fig. 10, proving that our system and algorithm are an effective way to monitor greenhouse gases, indirectly.

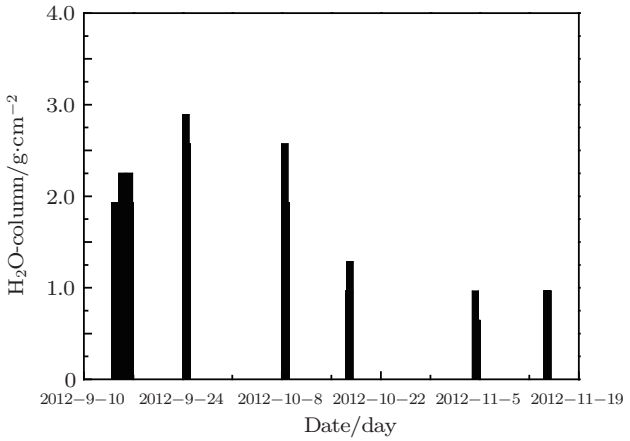


Fig. 9. Time series of retrieved 1-hour averaged values of H_2O columns from spectra measured by LRFTS in Hefei.

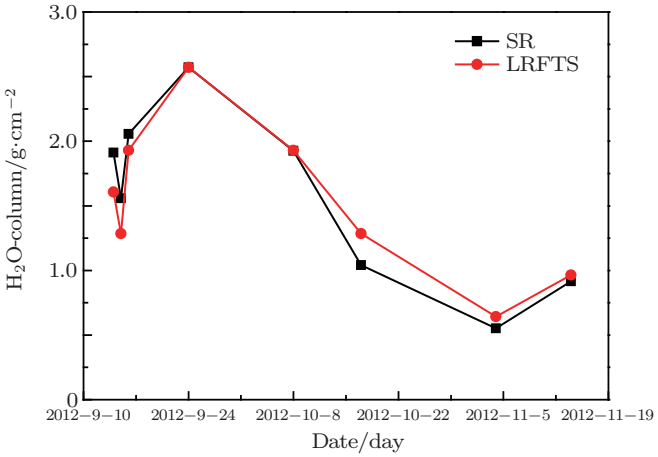


Fig. 10. (color online) Time series of H_2O columns retrieved from measured spectra by LRFTS and SR.

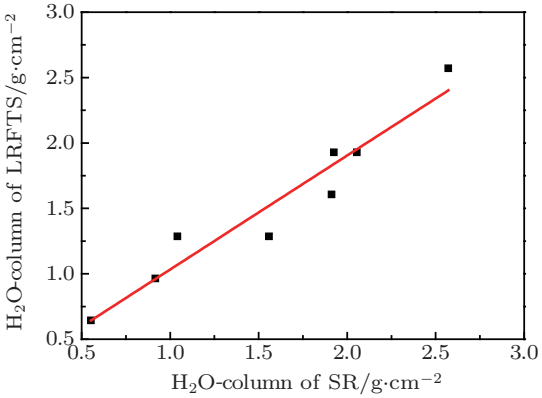


Fig. 11. (color online) The H_2O column linear fitting between LRFTS and SR, expressed by $y = 0.87x + 0.16$.

5. Conclusion

We developed a ground-based low-resolution Fourier transform spectrometry for the remote sensing of the total columns of CO_2 and CH_4. The observation was carried out

in Hefei automatically. This system has the advantages of low cost and portability compared with the high spectral resolution ones. The spectral inversion algorithm consists of three steps. Firstly, the atmospheric transmittance spectrum is computed line-by-line in the forward model based on the assumed atmospheric model. Secondly, the real atmospheric transmittance is observed from direct solar radiation with the pre-processing of spectral calibration by the Smithsonian long method. Finally, the total columns are calculated by nonlinear least squares fitting algorithm between the measured transmittance and modeled transmittance spectra in the backward model.

There are systematic deviations in the vertical columns of O_2, CO_2, and CH_4 inversed from total atmospheric observation transmittance spectra. These deviations maybe originate from the assumed atmospheric model, different spectral resolution, and the uncertainty of instrumental line shape. Column averaged dry-air mole fractions of CO_2 and CH_4 are measured with accuracies of 3.7% and 5% using the O_2 column as internal standard function, respectively. To verify the results, the vertical column of H_2O obtained by our system and that by the solar radiometer at the same site are compared. The correlation coefficient is 0.92, although there are some discrepancies on some days. This means that they accord very well with each other. Therefore the system and method are promising to become an important part of three-dimensional greenhouse gas monitoring, especially for local sources and field application.

References

[1] Wunch D, Toon G C, Blavier J F L, Washenfelder R A, Notholt J, Connor B J, Griffith D W T, Sherlock V and Wennberg P O 2011 *Phil. Trans. R. Soc. A* **369** 2087

[2] Thompson D R, Benner D C, Brown L R, Crisp D, Devi V M, Jiang Y B, Natraj V, Oyafuso F, Sung K, Wunch D, Castano R and Miller C E 2012 *J. Quant. Spectrosc. Radiat. Transfer* **113** 2265

[3] Reuter M, Bovensmann H, Buchwitz M, Burrows J P, Connor B J, Deutscher N M, Griffith D W T, Heymann J, Keppel-Aleks G, Messerschmidt J, Notholt J, Petri C, Robinson J, Schneising O, Sherlock V, Velazco V, Warneke T, Wennberg P O and Wunch D 2011 *J. Geophys. Res.* **116** D04301

[4] Dils B, Maziere M D, Muller J F, Blumenstock T, Buchwitz M, Beek R, Demoulin P, Duchatelet P, Fast H, Frankenberg C, Gloudemans A, Grifith D, Jones N, Kerzenmacher T, Kramer I, Mahieu E, Mellqvist J, Mittermeier R L, Notholt J, Rinsland C P, Schrijver H, Smale D, Strandberg A, Straume A G, Stremme W, Strong K, Sussmann R, Taylor J, Broek M, Velazco V, Wagner T, Warneke T, Wiacek A and Wood S 2006 *Atmos. Chem. Phys.* **6** 1953

[5] Geibel M C, Messerschmidt J, Gerbig C, Blumenstock T, Chen H, Hase F, Kolle O, Lavric J V, Notholt J, Palm M, Rettinger M, Schmidt M, Sussmann R, Warneke T and Feist D G 2012 *Atmos. Chem. Phys.* **12** 8763

[6] Wunch D, Toon G C, Wennberg P O, Wofsy S C, Stephens B B, Fischer M L, Uchino O, Abshire J B, Bernath P, Biraud S C, Blavier J F L, Boone C, Bowman K P, Browell E V, Campos T, Connor B J, Daube B C, Deutscher N M, Diao M, Elkins J W, Gerbig C, Gottlieb E, Griffith D W T, Hurst D F, Jimenez R, Aleks G K, Kort E A, Macatangay R, Machida T, Matsueda H, Moore F, Morino I, Park S, Robinson J, Roehl C M, Sawa Y, Sherlock V, Sweeney C, Tanaka T and Zondlo M A 2010 *Atmos. Meas. Tech.* **3** 1351

[7] Oshchepkov S, Bril A, Yokota T, Yoshida Y, Blumenstock T, Deutscher N M, Dohe S, Macatangay R, Morino I, Notholt J, Rettinger M, Petri C, Schneider M, Sussman R, Uchino O, Velazco V, Wunch D and Belikov D 2013 *Appl. Opt.* **52** 1339

[8] Cogan A J, Boesch H, Parker R J, Feng L, Palmer P I, Blavier J F L, Deutscher N M, Macatangay R, Notholt J, Roehl C, Warneke T and Wunch D 2012 *J. Geophys. Res.* **117** D21301

[9] Petri C, Warneke T, Jones N, Ridder T, Messerschmidt J, Weinzierl T, Geibel M and Notholt J 2012 *Atmos. Meas. Tech. Discuss.* **5** 245

[10] Fu D J, Sung K, Boone C D, Walker K A and Bernath P F 2008 *J. Quant. Spectrosc. Radiat. Transfer* **109** 2219

[11] Liu Z M, Liu W Q, Gao M G, Tong J J, Zhang T S, Xu L, Wei X L, Jin L, Wang Y P and Chen J 2010 *Acta Phys. Sin.* **59** 5397 (in Chinese)

[12] Liu Z M, Liu W Q, Gao M G, Tong J J, Zhang T S, Xu L and Wei X L 2008 *Chin. Phys. B* **17** 4184

[13] Wang Y, Xie P H, Li A, Zeng Y, Xu J and Si F Q 2012 *Acta Phys. Sin.* **61** 114209 (in Chinese)

[14] Xu J, Xie P H, Si F Q, Li A and Liu W Q 2012 *Acta Phys. Sin.* **61** 024204 (in Chinese)

[15] Yang Z H, Toon G C, Margolis J S and Wennberg P O 2002 *Geophys. Res. Lett.* **29** 1339

[16] Zou M M, Fang Y H, Xiong W and Shi H L 2009 *Acta Opt. Sin.* **29** 1701 (in Chinese)

[17] Guo R P, Zhan J and Rao R Z 2006 *Chin. J. Quan. Elec.* **23** 736 (in Chinese)

[18] Liou K N 2002 *An Introduction to Atmospheric Radiation*, 2nd edn. (California: Academic Press Inc.) p. 57

[19] Dufour E, Breon F M and Peylin P 2004 *J. Geophys. Res.* **109** D09304

[20] Mao J P and Kawa S R 2004 *Appl. Opt.* **43** 914

[21] Heymann J, Schneising O, Reuter M, Buchwitz M, Rozanov V V, Velazco V A, Bovensmann H and Burrows J P 2012 *Atmos. Meas. Tech.* **5** 1935

[22] Gisi M, Hase F, Dohe S, Blumenstock T, Simon A and Keens A 2012 *Atmos. Meas. Tech.* **5** 2969

[23] Hase F 2012 *Atmos. Meas. Tech.* **5** 603

[24] Liu Y, Wang X F, Guo M and Tani H 2012 *Int. J. Remote Sens.* **33** 3004